

# Kinetic traps in chemically fueled self-assembly and how to overcome them.

Brigitte A. K. Kriebisch\*, Christine M. E. Kriebisch\*, Alexander M. Bergmann, Caren Wanzke, Marta Tena-Solsona, Job Boekhoven

**KEYWORDS** *Kinetically trapping – Microenvironmental change –  $pK_a$  Shift – Disassembly – Dynamic Fibers.*

---

**ABSTRACT:** Nature uses dynamic, molecular self-assembly to create cellular architectures that adapt to their environment. For example, a guanosine triphosphate (GTP)-driven reaction cycle activates and deactivates tubulin for assembly into microtubules and disassembly. Inspired by dynamic self-assembly in biology, multiple studies have developed synthetic analogs of assemblies regulated by chemical chemically fueled reaction cycles. A challenge in most of these studies is that molecules assemble upon activation but do not disassemble upon deactivation. In other words, they remain kinetically trapped, and the resulting assemblies are not dynamic. In this work, we show how molecular design dictates the tendency of deactivated molecules to remain trapped in the assembled state. We also show how molecular design can be used to tune the dynamics of the reaction cycle. Our work should result in chemically fueled assemblies that are truly dynamic in that disassembly immediately follows deactivation.

---

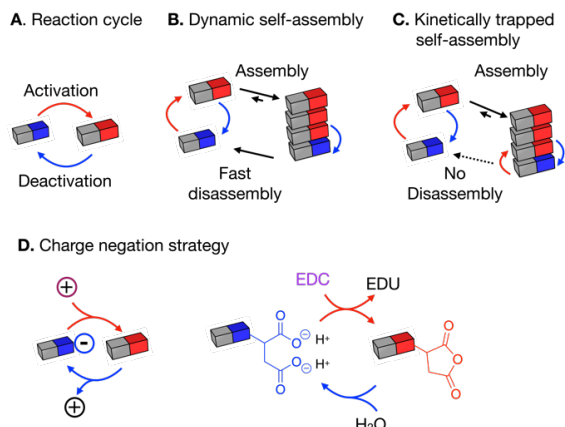
**Introduction.** In molecular self-assembly, molecules are designed to interact with one another to form larger, supramolecular complexes.<sup>1-4</sup> The assembly process alters the material properties of the system, which gives rise to supramolecular materials.<sup>5-9</sup> In recent years, there has been a focus on dynamic supramolecular materials, *i.e.*, materials that change and adapt to their environment.<sup>10-12</sup> In such materials, molecules are designed to assemble or disassemble in response to a trigger. For example, peptides can be designed to assemble or disassemble upon enzymatic phosphorylation, dephosphorylation, or an increase in pH.<sup>13-15</sup> In these dynamic assembly mechanisms, kinetic traps can occur those trap molecules in their assembly because the thermal energy available is insufficient to overcome the energy barrier for disassembly.<sup>16-18</sup> As molecules and their assembly become increasingly more complex; it becomes more challenging to predict whether such unwanted kinetic trapping will occur.

Chemically fueled self-assembly is an extreme case of dynamic self-assembly in which kinetic trapping is particularly unwanted.<sup>19-21</sup> Here, assembly is coupled to a chemical reaction cycle to yield assemblies regulated through the kinetics of that reaction cycle. The reaction cycle comprises at least two chemical reactions, *i.e.*, an activation reaction that activates building blocks for self-assembly at the expense of a high-energy chemical reagent (*i.e.*, a chemical fuel) and a spontaneous deactivation reaction reverts the building blocks to their precursor state (Scheme 1A). In dynamic self-assembly of, for example, tubulin or actin, the emerging assemblies have vastly different properties compared to their in-equilibrium analogs because building blocks are constantly activated and deactivated for assembly.<sup>22</sup> When the assembly and

disassembly rates of building blocks are fast, the assemblies are dynamic, and their properties are regulated through the kinetics of the reaction cycle resulting in exciting behavior like treadmilling and size control (Scheme 1B).

In contrast, when disassembly of the precursor is slow, the molecules remain trapped in the assembled state and can reactivate before disassembly. Such a situation results in chemically fueled self-assembly without the dynamics of assembly and disassembly. It is to a much lesser degree, regulated by the kinetics of the reaction cycle (Scheme 1C). In other words, the exciting properties of chemically fueled self-assembly are lost when disassembly is slow. To design molecules that are rapidly disassembling after deactivation remains a challenge because the mechanisms of kinetic trapping are poorly understood.

**Scheme 1. A)** Scheme of a fuel-driven reaction cycle. Red arrows depict fuel-driven activation reactions. Blue arrows depict spontaneous deactivation reactions. **B)** In chemically fueled, dynamic self-assembly, the activated building block should assemble while the deactivated building block disassembles. **C)** In kinetically trapped assemblies, disassembly does not follow deactivation. Building blocks get reactivated in the assembly. **D)** Transient negation of charges by the reaction cycle can be applied to drive self-assembly. EDC-driven reaction cycle negates the charges on a dicarboxylate.



To create chemically fueled assemblies, we and others used a strategy in which a chemical reaction cycle transiently negates the charges on a molecule (Scheme 1D).<sup>22-41</sup> Upon activation, an anionic, well-soluble precursor becomes charge-neutral, which induces product assembly. The deactivation occurs while the building block is assembled; it reinstates the negative charges and thus leads to its disassembly. We described a reaction cycle driven by the hydration of the condensing agent EDC (1-ethyl-3-(3-dimethyl aminopropyl)carbodiimide, Scheme 1D).<sup>26</sup> In the activation, EDC reacts with an anionic dicarboxylate precursor to form its corresponding uncharged anhydride (product). In the deactivation, the product hydrolyzes to yield the dicarboxylate precursor. The anhydride precursor has a half-life of tens of seconds before deactivation. The removal of the charges of the anionic dicarboxylate can induce self-assembly. *Vice versa*, the deactivation converts the non-charged anhydride to its corresponding dicarboxylate *via* hydrolysis and yields the charged precursors, which induces disassembly.

Using the charge abolishment approach has resulted in assemblies with dynamic behavior like vesicles<sup>30</sup>, coacervates<sup>28</sup>, and oil droplets<sup>42</sup>. However, not all fueled assemblies formed through charge negation are dynamic. In some cases, chemically fueled self-assembly into fibers results in slow disassembly or even kinetically trapped assemblies.<sup>26, 29, 31</sup> In other words, the dynamics of the reaction cycle are fast, but the dynamics of assembly and disassembly are not. Furthermore, because the mechanisms of kinetic trapping are not understood, it is challenging to predict or design molecules that form dynamic assemblies.

In this work, we study the mechanism of kinetically trapping in chemically fueled fibers regulated through transient charge negation. We find that the assembly increases the peptide's apparent  $pK_a$ , which implies that the molecule remains protonated upon deactivation. In its protonated, uncharged state, the charge-charge repulsion with neighboring deactivated precursors is negligible, which explains why the disassembly is slow, and precursors remain trapped. We believe this mechanism is generalizable for the disassembly of other peptides based on charge-charge repulsion.<sup>31, 41, 43-44</sup> We also provide solutions to overcome the trapping of the precursor in the fibers, which yield chemically fueled fibers with increased dynamics.

## Results and Discussion.

**Molecular design controls kinetic trapping.** We used the tripeptides Fmoc-GGD and Fmoc-AVD (Fig. 1A, B), where G is the amino acid glycine, A is the amino acid alanine, and V is the amino acid valine, and D stands for aspartic acid. These peptides are dissolved at 10 mM in an aqueous buffer of MES at pH 6.0. A Nile Red assay found no evidence of assembly, confirming that these peptides were well-dissolved in their precursor state (Fig. 1C, D, Fig. S1). The addition of 100 mM EDC to these precursor solutions initiated the reaction cycle. It led to the formation of a turbid solution and a turbid hydrogel for Fmoc-GGD and Fmoc-AVD, respectively. Notably, the turbidity by Fmoc-GGD was transient and faded as the reaction cycle had consumed all fuel. In contrast, the hydrogel of Fmoc-AVD was not transient and remained intact far after all fuel was consumed (Fig. 1C-F). Confocal microscopy was used to study the morphology of the assembly and found, in line with previous work, that Fmoc-GGD formed transient vesicles,<sup>26</sup> whereas Fmoc-AVD assembled into fibers (Fig. 1C, D).<sup>30</sup> We studied the evolution of the reaction cycle by applying fuel, and at predetermined time points, we used a benzylamine quench<sup>45</sup> to stop the reaction cycle and measure its contents by HPLC (Fig. 1E, F). The anhydride product was temporarily present, and, as the system was running out of fuel, the product disappeared.

To assess the dynamics of the assembly and disassembly process, the turbidity of the solution in response to EDC was followed in a plate reader (Fig. 1E, F). While the Fmoc-GGD-based vesicles dissolved to yield a transparent solution as the product concentration decayed, the fibers by Fmoc-AVD did not. After 24 hours, a substantial amount of turbidity was observed for Fmoc-AVD, despite all anhydride having hydrolyzed within the first hour of the reaction cycle. From this observation, it is clear that the precursor remained kinetically trapped in the fibers.

Using <sup>1</sup>H-NMR spectroscopy, the assembly's composition was measured as a function of time. We used the fact that peptides in an assembly become NMR-silent. We can thus measure how much of the 10 mM initial peptide resides in the assemblies. Combined with the concentrations of the activated product as determined by HPLC, we could thus determine the ratio of precursor and product in the assemblies. Here we assume that all activated product is in the assemblies. Three minutes after the addition of EDC, we found that both the fibers and the vesicles were composed of a coassembly of precursor and product (Fig. S2). However, 24 hours after starting the reaction cycle, we found no more NMR-silent peptide in the case of Fmoc-GGD, which points to complete disassembly. In contrast, for Fmoc-AVD, roughly 4.3 mM precursor remained kinetically trapped in assemblies (Fig. 1G). Only by annealing the kinetically trapped Fmoc-AVD at 95°C for 5 min, we could dissolve the precursor (Fig. S3). Finally, we supported our finding that Fmoc-AVD is kinetically trapped by a Nile Red assay. The Nile Red emission remained high for Fmoc-AVD, whereas no emission signal was visible for Fmoc-GGD after 24 hours (Fig. 1H).

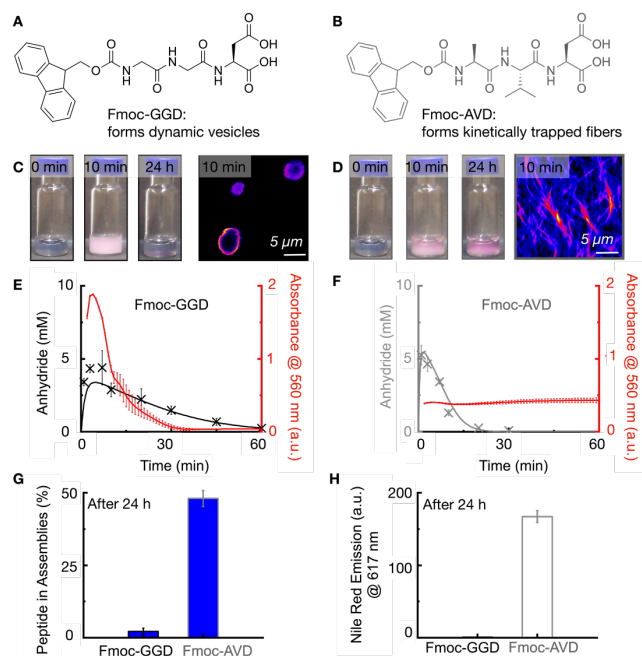


**Figure 1.** Peptide design controls kinetic trapping after the application of fuel. **A-B)** Molecular structure of Fmoc-GGD and Fmoc-AVD. **C-D)** Photographs and confocal micrographs, after fueling 10 mM of **C)** Fmoc-GGD and **D)** Fmoc-AVD with 100 mM EDC, stained with 25  $\mu$ M Nile Red dye. Scale bar 5  $\mu$ m. **E-F)** Indication of correlation between the assembly process and the kinetics by measuring the anhydride formation (black markers) and the absorbance at 560 nm (solid red line) when fueling **E)** 10 mM Fmoc-GGD, and **F)** 10 mM Fmoc-AVD with 100 mM EDC, stained with 25  $\mu$ M Nile Red dye. A kinetic model was used to fit the experimental data (solid black line, Supporting Notes). **G)** The percentage of trapped precursor in the molecular assemblies after 24 hours, when 10 mM Fmoc-GGD, and 10 mM Fmoc-AVD were fueled with 100 mM EDC as determined by  $^1$ H-NMR spectroscopy. **H)** Maximum emission intensity of Nile Red (a.u.) at 617 nm, 24 hours after fueling 10 mM Fmoc-GGD (hardly visible), 10 mM Fmoc-AVD with 100 mM EDC. All error bars are the standard deviation of the mean ( $n = 3$ ).

### The mechanism that kinetically traps precursors

In the chemically fueled assemblies design through the charge abolishment strategy, we reasoned that the negatively charged precursors repel each other to overcome the attractive forces that lead to their disassembly. Based on the above data, this is not the case. We hypothesized that the precursor in the assembly might not be as anionic as we initially suspected. Upon deactivation of the product in a fiber of Fmoc-AVD, the negative charges on the precursor's carboxylate are not reinstated. This mechanism is induced by a drastic shift in the  $pK_a$  in the microenvironment of the fiber.<sup>29</sup> In other words, the precursor in solution is deprotonated, which prevents its assembly. However, it remains (partially) protonated in the fiber, and thus charge neutral and unable to disassemble (Fig. 2A). We measured the  $pK_a$  of the Fmoc-AVD, and Fmoc-GGD and compared Ac-FAVD, a peptide that does not assemble and has  $pK_a$ 's of 2.2 and 4.2 (Fig. 2A, Fig. S4). For Fmoc-GGD, we found only one  $pK_a$  at 4.4 by titration of HCl. Interestingly, when the pH was close to the  $pK_a$ , the

solution turned turbid. In other words, the measured  $pK_a$  was of the precursor in an assembled state, which was likely different than the  $pK_a$  of the precursor in solution. In contrast, for Fmoc-AVD, we found a  $pK_a$  of 5.8, *i.e.*, far higher than the non-assembling Ac-FAVD (Fig. 2A, Fig. S4).

As we carry out our chemically fueled reaction cycle at pH 6.0, it is reasonable to assume that most of the precursor of Fmoc-GGD in the solution or in the vesicles is completely deprotonated. In the case of Fmoc-AVD, the  $pK_a$  in the fibers is close to experimental conditions, which implies that, on average, less than half of the carboxylates were deprotonated in the fibers. Consequently, the driving force of disassembly, *i.e.*, the accumulation of negative charges on the precursor, is far less prevalent on Fmoc-AVD than Fmoc-GGD. To further corroborate that hypothesis, we monitored the chemically fueled fibers by confocal microscopy in combination with Hoechst dye 33258. That dye is cationic and stains anionic assemblies like proteins and peptides, enabling us to monitor the accumulation of negative charges (Fig. S5).<sup>46</sup> We found that Hoechst 33258 colocalized with the vesicles formed by Fmoc-GGD throughout the reaction cycle (Fig. 2B). In contrast, the fibers formed by Fmoc-AVD hardly incorporated some Hoechst 33258 dye at the beginning of the reaction cycle, when deactivation is at its highest. After 10 min, the Hoechst 33258 signal was very faint or not observable, from which we conclude that the fibers are hardly anionic, which corroborates our earlier findings (Fig. 2B). Finally, we performed the same experiments described above, but at various pH values between pH 6.0 and 6.5.  $^1$ H-NMR showed a clear trend that less precursor got trapped with increasing pH, further corroborating that the pH of the surrounding media is not sufficient to deprotonate the kinetically trapped precursor (Fig. 2C, Fig. S6-8). We assume that working above pH 6.5 would further avoid the kinetic trapping precursor. However, at pH 7 or higher, we observed the formation of significant amounts of the side product N-acylisourea and much less anhydride.

### The flat packing of $\beta$ -sheets is responsible for the $pK_a$ -shift.

We explain the  $pK_a$  difference between assemblies of Fmoc-AVD and Fmoc-GGD by valine's high propensity to form flat  $\beta$ -sheets compared to glycine. The formation of these flat  $\beta$ -sheets implies that the C-terminal aspartic acids are packed in a relatively high density known to shift  $pK_a$ s.<sup>47,47-48</sup> We measured the assembly's ability to bind Thioflavin (ThT), which measures the flatness of  $\beta$ -sheets.<sup>49,50</sup> We measured a high ThT signal when we fueled Fmoc-AVD with EDC, while we found no significant emission of ThT when we fueled Fmoc-GGD with EDC (Fig. 2D). Fourier-Transform Infrared Spectroscopy (FT-IR) revealed that both peptides had two predominant peaks around 1690  $cm^{-1}$  and 1630  $cm^{-1}$ , which we assign to the Fmoc-OCNH band and the amide I band (Fig. 2E). The amide I band (carbonyl stretch vibration) is particularly sensitive to hydrogen bonding in the peptide assembly.<sup>51-52</sup> For Fmoc-AVD, this peak was located at 1632  $cm^{-1}$  and relatively sharp, which is indicative of elements of  $\beta$ -sheet (1625  $cm^{-1}$ – 1640  $cm^{-1}$ ).<sup>53</sup> The same peak for Fmoc-GGD

broadened drastically and shifted towards the region of  $1650\text{ cm}^{-1}$ , which points towards elements of a random coil ( $1640\text{ cm}^{-1}$ –  $1650\text{ cm}^{-1}$ ). The FT-IR data further corroborate that Fmoc-GGD is mainly engaged in random coil hydrogen bonds, whereas flat  $\beta$ -sheets are present in Fmoc-AVD assemblies. These flat  $\beta$ -sheets pack the carboxylates closely such that their  $pK_a$ s shift.

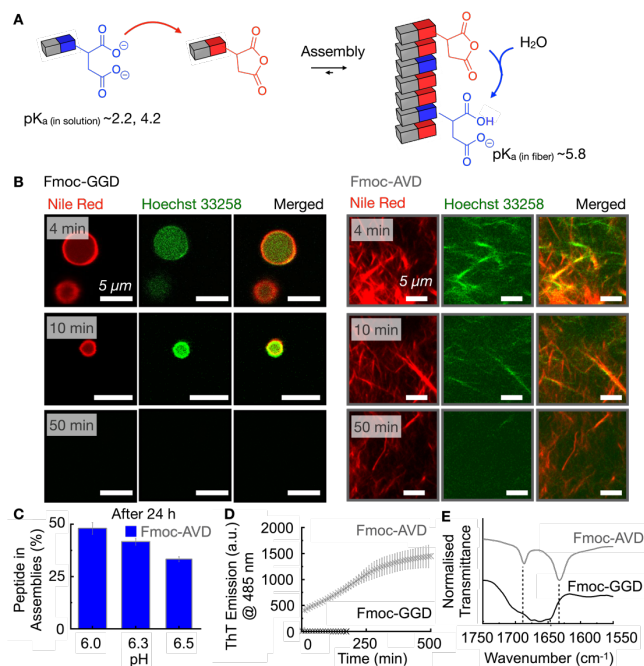


**Figure 2. The mechanism of kinetic trapping.** **A)** The  $pK_a$  of aspartic acid depends strongly on its microenvironment. **B)** Confocal micrographs after fueling 10 mM of Fmoc-GGD, 10 mM of Fmoc-AVD with 100 mM EDC, stained with  $25\ \mu\text{M}$  Nile Red and  $25\ \mu\text{M}$  Hoechst 33258 dye, respectively. Scale bar  $5\ \mu\text{m}$ . **C)** The percentage of trapped precursor in the molecular assemblies after 24 hours when 10 mM Fmoc-AVD were fueled with 100 mM EDC at pH 6, pH 6.3, and pH 6.5 as determined by  $^1\text{H-NMR}$  spectroscopy. **D)** ThT fluorescence intensity at 485 nm over time as a measure of the presence of  $\beta$ -sheets when 1 mM Fmoc-AVD or 1 mM Fmoc-GGD are fueled with 100 mM EDC, respectively. **E)** FTIR spectra of 10 mM Fmoc-AVD or 10 mM Fmoc-GGD fueled with 100 mM EDC at 3 min. The Fmoc-OCNH band at  $1687\text{ cm}^{-1}$  and amide I band at  $1632/1647\text{ cm}^{-1}$  (typical  $\beta$ -sheet) for Fmoc-AVD/Fmoc-GGD. All error bars represent the standard deviation of the mean for  $n = 3$ .

To test which of the amides in the peptide contributed to the organization of the C-termini and thus the shift in  $pK_a$  and kinetic trapping, we synthesized Fmoc-AVD(NMe) (Fig. 3). This compound is similar to Fmoc-AVD but lacks the last NH-bond due to methylation, which shifted the  $pK_a$  from 5.8 to 4.2 (Fig. 3, Fig. S9). In other words, the  $pK_a$ -shift upon self-assembly had disappeared entirely. Furthermore, transient aggregates emerge upon fueling 10 mM Fmoc-AVD(NMe) with 100 mM EDC (Fig. S10).  $^1\text{H-NMR}$  and HPLC studies on the reaction cycle of Fmoc-AVD(NMe) showed a complete lack of coassembly of the precursor and thus also no kinetic trapping (Fig. S10). In other words, methylation of this crucial amide means that the precursor does not coassemble, and we can recover

the dynamic character of the chemically fueled self-assembly.

Compound	H-bonding interaction	$pK_a$	Chemical structure
Fmoc-AVD(NMe)	Non	$\sim 4.2 \pm 0.1$ $\sim 4.2 \pm 0.1$	
Fmoc-GGD	Weak	$\sim 4.4 \pm 0.1$ $\sim 4.4 \pm 0.1$	
Fmoc-AVD	Strong	$\sim 5.8 \pm 0.1$ $\sim 5.8 \pm 0.1$	

**Figure 3.** H-bonding of aspartic acid NH controls the  $pK_a$  shift. Schematic representation of H-bonding interaction of aspartic acid NH bond in Fmoc-AVD(NMe), Fmoc-GGD, and Fmoc-AVD assemblies.  $pK_a$  change of aspartic acid residue depends strongly on the H-bonding interaction strength of the aspartic acid NH-bond, *i.e.*, the stronger the H-bonding interaction, the higher the  $pK_a$  value.

### Recovering chemically fueled self-assembly

We explored whether we could tune the degree of kinetically trapping of precursors in fibers by mixing Fmoc-AVD with Fmoc-GGD. We assume that both peptides coassemble and form weaker hydrogen bonds resulting in a milder shift in the  $pK_a$  of the carboxylates, thereby increasing the amount of negatively charged precursor molecules per fiber. Cryogenic transmission electron microscopy (cryo-TEM) showed that Fmoc-GGD assembled into vesicles in response to fuel (Fig. 4A), while a mixture of 25 mol% of Fmoc-AVD and 75 mol% Fmoc-GGD resulted in twisted tapes instead of vesicles; a good indication that the two coassemble. Moreover, the tapes of the mixture were more twisted compared to the tapes formed by 100 mol% Fmoc-AVD, which we explain by the decrease in the ability to form flat  $\beta$ -sheets. Indeed, a ThT-assay showed that the maximum emission intensity observed after the addition of EDC declined with the increasing ratio of Fmoc-GGD to Fmoc-AVD (Fig. 4B; Fig. S11). This observation was further corroborated by the center of the amide-I band shifting from  $1632\text{ cm}^{-1}$  to  $1647\text{ cm}^{-1}$  upon gradually increasing the ratio of Fmoc-GGD to Fmoc-AVD (Fig. 4C, Fig. S12). More excitingly, the decrease in  $\beta$ -sheet's rigidity enabled us to tune the  $pK_a$  of the precursor between 5.8 and  $pK_a$  4.4 (Fig. 4D, Fig. S4). Thus, tuning the peptide content allowed us to change the microenvironment of the precursor and, with that, its degree of deprotonation.  $^1\text{H-NMR}$  and fluorescence spectroscopy confirmed a decrease of kinetically trapped precursor from 48% to 18% for pure Fmoc-AVD to 50 mol% Fmoc-AVD with Fmoc-GGD content (Fig. 4E, Fig. 5A-C, Fig. S13).

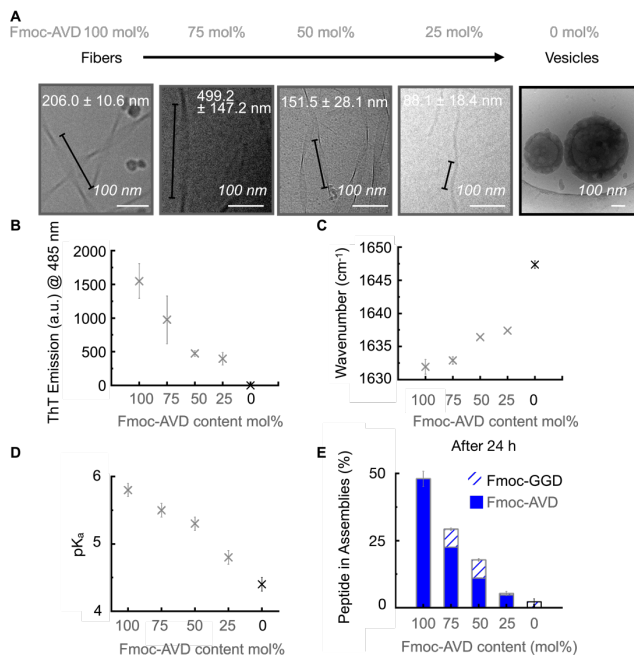
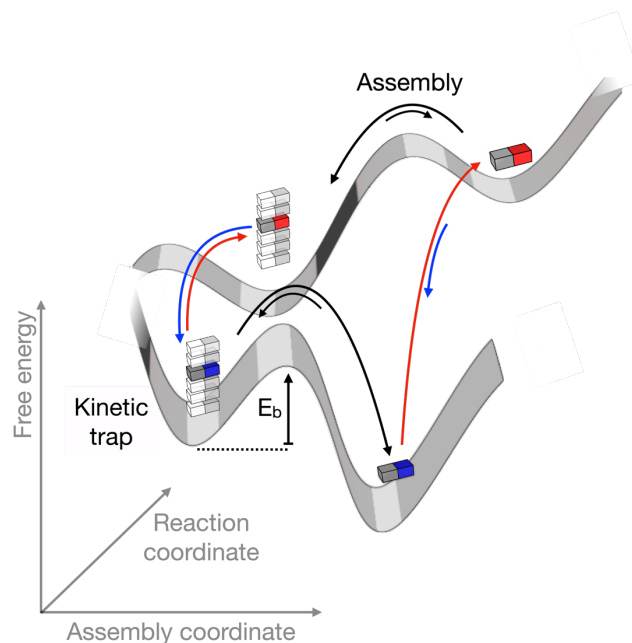


**Figure 4.** Changing the precursor's microenvironment through coassembly. **A)** Cryo-TEM micrographs of 10 mM peptide solutions with varying Fmoc-AVD and Fmoc-GGD composition, 2 minutes after fueling with 10 mM EDC; for 100 mol% Fmoc-GGD 4 minutes after fueling with 50 mM EDC. Scale bar 100 nm. **B)** The maximum ThT emission (a.u.) at 485 nm after excitation at 440 nm of 1 mM peptide solution with varying Fmoc-AVD and Fmoc-GGD composition. These solutions are fueled with 100 mM EDC. **C)** Maximum IR-absorption wavenumber of amide I derived from FT-IR spectra of 10 mM peptide solution with varying ratios of Fmoc-AVD and Fmoc-GGD. The solutions were fueled with 100 mM EDC, and spectra were recorded after 3 minutes. **D)** The pK<sub>a</sub> values of the carboxylates of the peptides in assemblies for 10 mM total peptide concentration. **E)** The percentage of trapped precursors in the molecular assemblies after 24 hours as determined by <sup>1</sup>H-NMR. All solutions contained 10 mM peptide with varying Fmoc-AVD and Fmoc-GGD composition and were fueled with 100 mM EDC. All error bars represent the standard deviation of the mean for n = 3.

From the combined experiments, we can create a simplified energy landscape of the transitions occurring in our chemically fueled system (Scheme 2). The peptide in this landscape can be in four states: it can be activated or not, and it can be in solution or the microenvironment of the fiber. Consequently, four reversible transitions are possible, *i.e.*, the non-assembled precursor can be activated, the activated building block can assemble, the assembled activated product can deactivate, and the deactivated precursor can disassemble. The thermodynamically most favored state is the non-activated, non-assembled peptide. Upon activation, the product assembles into a fiber. Deactivation leads to the deactivated peptide in a fiber. The disassembly of the precursor is endowed with a high energy barrier ( $E_b$ ) which leads to the precursor being kinetically trapped within the fiber. Due to the kinetic trapping, the deactivated peptide is more likely to become re-activated than disassemble. Thus, the peptide spends most of its time in the peptide microenvironment, and this is

also where most fuel is consumed. Through changes in molecular design and pH, the  $E_b$  can be decreased.

**Scheme 2.** Schematic and simplified representation of the free energy landscape of chemically fueled assembly.



With our increased understanding of trapping in chemically fueled assembly, we tested the dynamics of assemblies by measuring the amount of peptide in the assembly as a function of time using <sup>1</sup>H-NMR spectroscopy (Fig. 5 A-C). For assemblies of Fmoc-AVD fueled with 100 mM EDC at pH 6 and 6.5, we found that 66% and 60% of peptide remained in the assembly one hour after EDC addition. For assemblies of 50 mol% Fmoc-AVD and 50 mol% Fmoc-GGD at pH 6, trapped assembled peptide decreased to 30%. We used confocal microscopy to study the dynamics of assembly and disassembly further. We imaged several XYZ-stacks (z-dimension 5-10  $\mu\text{m}$ ) over time. After imaging the temporal z-stacks, we corrected for x/y-drift. We analyzed the change of the images as a function of time by calculating the Pearson correlation coefficient between sequential images of an area of 8.7  $\mu\text{m}$  x 10.2  $\mu\text{m}$ . We calculated the Pearson correlation coefficient between frames spaced apart 10 min (Fig. 5D-F). For assemblies of Fmoc-AVD at pH 6, the Pearson correlation coefficient ranges between 0.9 and 1.0 (Fig. 5D, G). A strong correlation from image to image implies a lack of assembly and disassembly. At pH 6.5, the correlation coefficient ranged from 0.75 and 1.0, which shows that the assemblies were slightly more dynamic (Fig. 5E, H). Finally, for assemblies of 50 mol% Fmoc-AVD and 50 mol% Fmoc-GGD at pH 6, the range of the correlation coefficient broadened to 0.25-1.0, indicating that these assemblies are more dynamic than pure Fmoc-AVD (Fig. 5F, I).

Excitingly, we observed behavior reminiscent of the dynamic instabilities of microtubules, *i.e.*, some fibers could switch from growing to collapsing and back to growing again. This behavior was only observed on fiber ends that were not embedded in a dense network of other fibers

making it complicated to image these fibers due to the drifting of the sample. Thus, we trapped 2.5 mM of precursor solution in a 1.5% agarose gel and added a layer of 100 mM EDC on top of the gel. Doing ensured the fibers were in a pseudo-steady state (Fig. S14-15) and tended to drift less. We imaged the samples and followed the evolution of a fiber's length as a function of time over several z-planes (5-10  $\mu\text{m}$ ). For Fmoc-AVD at pH 6 or pH 6.5, no noticeable growth and collapse of the dangling fibers were found (Fig. 5J). For the mixture of 50 mol% Fmoc-GGD and 50 mol% Fmoc-AVD assemblies, some fiber tips alternately grew and collapsed while fuel was present (Fig. 5J, K). 3D projections of the images confirmed that the fibers were not falling in and out of the focal plane but growing and shrinking (Fig. 5K, L, Fig. S16-17, Supporting Movie M1-4). From the data in Fig. 5C and Fig. S16-17, it can be noted that fibers grow and collapse on a time scale of 0.1 - 1.4  $\mu\text{m}/\text{min}$ .

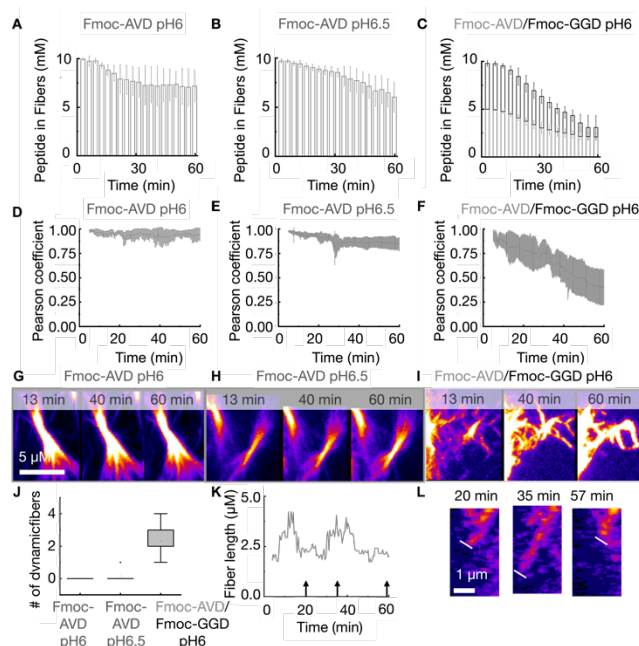


**Figure 5.** Dynamic self-assembly of fibers. **A-C)** The concentration of peptide in the assemblies as a function of time determined by  $^1\text{H-NMR}$  spectroscopy for 10 mM Fmoc-AVD at pH 6 (**A**) and pH 6.5 (**B**) and 5 mM Fmoc-AVD mixed with 5 mM Fmoc-GGD at pH 6 (**C**), all fueled with 100 mM EDC. **D-F)** The correlation coefficient between two confocal micrographs taken 10 minutes apart as a function of time. The following conditions were used: 10 mM Fmoc-AVD at pH 6 (**D**) or pH 6.5 (**E**) and 5 mM Fmoc-AVD mixed with 5 mM Fmoc-GGD at pH 6 (**F**) all fueled with 100 mM EDC. **G-I)** Confocal micrographs, 13 min, 40 min, and 60 min after fueling. The conditions were: **G)** 10 mM Fmoc-AVD at pH 6, **H)** 10 mM Fmoc-AVD at pH 6.5 and **I)** 5 mM of Fmoc-GGD mixed with 5 mM of Fmoc-AVD at pH 6 with 100 mM EDC, stained with 25  $\mu\text{m}$  Nile Red. Scale bar 5  $\mu\text{m}$ . **J)** Number of counted dynamic fibers that grow and collapse in (18x12  $\mu\text{m}$ ). **K)** Fiber length as a function of time for a growing and shrinking fiber. The analyzed fiber is shown in **L)** and the supporting movie M1 and was obtained after fueling 1.25 mM of Fmoc-GGD mixed with 1.25 mM of Fmoc-AVD with 100 mM EDC at pH 6. Arrows highlight the time points confocal micrographs are shown in **L)**. **L)** Confocal micrographs 20 min, 35 min,

and 57 min after fueling 1.25 mM of Fmoc-GGD mixed with 1.25 mM of Fmoc-AVD with 100 mM EDC at pH 6, stained with 25  $\mu\text{m}$  Nile Red. Scale bar 1  $\mu\text{m}$ . All error bars represent the standard deviation of the mean for  $n = 3$ .

## Conclusion and Outlook

We demonstrated how precursors remain kinetically trapped in chemically fueled fibers regulated through transient charge negation. We provided solutions to overcome the trapping of the precursor in the fibers, which yield fibers with increased dynamics. The mechanism can be exploited to design fibers that show dynamic instabilities as microtubules do in future work.

## ASSOCIATED CONTENT

### Supporting Information

Materials and methods description and additional data on the characterization of precursor and product (ESI-MS, NMR, HPLC); fluorescence spectroscopy data; FT-IR spectroscopy data; kinetic data; confocal microscope images; titration data are provided as PDF file.

Supporting movies M1-4 of dynamic fibers captured with confocal microscopy are provided as AVI files.

## AUTHOR INFORMATION

### Corresponding Author

Job Boekhoven—Department of Chemistry, Technical University of Munich, 85748 Garching, Germany; orcid.org/0000-0002-9126-2430; Email: job.boekhoven@tum.de

### Authors

Brigitte A. K. Kriebisch—Department of Chemistry, Technical University of Munich, 85748 Garching, Germany; orcid.org/0000-0001-6551-7279

Christine M. E. Kriebisch—Department of Chemistry, Technical University of Munich, 85748 Garching, Germany; orcid.org/0000-0002-9713-0295

Alexander M. Bergmann—Department of Chemistry, Technical University of Munich, 85748 Garching, Germany

Caren Wanzke—Department of Chemistry, Technical University of Munich, 85748 Garching, Germany

Marta Tena-Solsona—Department of Chemistry, Technical University of Munich, 85748 Garching, Germany orcid.org/0000-0002-0717-2046

### Author Contributions

The manuscript was written through the contributions of all authors. All authors have approved the final version of the manuscript. \*These authors contributed equally.

### Notes

The authors declare no competing financial interest.

## ACKNOWLEDGMENT

The BoekhovenLab is grateful for support from the TUM Innovation Network - RISE funded through the Excellence Strategy. This research was conducted within the Max Planck School Matter to Life, supported by the German

Federal Ministry of Education and Research (BMBF) in collaboration with the Max Planck Society. B.A.K.K. is grateful for a Kekulé-Stipendium by the Verbandes der Chemischen Industrie. J.B. is grateful for funding from the European Research Council (ERC starting grant 852187), the Volkswagen Foundation via the Life? Program. Cryo-TEM measurements were performed using infrastructure contributed by the Dietz Lab and the TUM EM Core Facility. We acknowledge the technical support provided by Fabian Kohler.

## ABBREVIATIONS

Cryo-TEM, cryogenic transmission electron microscopy; EDC, 1-ethyl-3-(3-(dimethylamino)propyl)carbodiimide; ESI-MS, electrospray ionization–mass spectrometry; Fourier-Transform Infrared Spectroscopy (FT-IR); GTP, guanosine triphosphate; HPLC, high-performance liquid chromatography; MES, 2-(N-morpholino)-ethanesulfonic acid; Nuclear Magnetic Resonance spectroscopy, NMR.

## REFERENCES

- Krissanaprasit, A.; Key, C. M.; Pontula, S.; LaBean, T. H., Self-Assembling Nucleic Acid Nanostructures Functionalized with Aptamers. *Chem. Rev.* **2021**, *121* (22), 13797-13868.
- Zhu, J.; Avakyan, N.; Kakkis, A.; Hoffnagle, A. M.; Han, K.; Li, Y.; Zhang, Z.; Choi, T. S.; Na, Y.; Yu, C.-J.; Tezcan, F. A., Protein Assembly by Design. *Chem. Rev.* **2021**, *121* (22), 13701-13796.
- Sheehan, F.; Sementa, D.; Jain, A.; Kumar, M.; Tayarani-Najjaran, M.; Kroiss, D.; Ulijn, R. V., Peptide-Based Supramolecular Systems Chemistry. *Chem. Rev.* **2021**, *121* (22), 13869-13914.
- Song, Q.; Cheng, Z.; Kariuki, M.; Hall, S. C. L.; Hill, S. K.; Rho, J. Y.; Perrier, S., Molecular Self-Assembly and Supramolecular Chemistry of Cyclic Peptides. *Chem. Rev.* **2021**, *121* (22), 13936-13995.
- Aida, T.; Meijer, E. W.; Stupp, S. I., Functional supramolecular polymers. *Science* **2012**, *335* (6070), 813-7.
- Amabilino, D. B.; Smith, D. K.; Steed, J. W., Supramolecular materials. *Chem. Soc. Rev.* **2017**, *46* (9), 2404-2420.
- Chen, H.; Fraser Stoddart, J., From molecular to supramolecular electronics. *Nat. Rev. Mater.* **2021**, *6* (9), 804-828.
- Boekhoven, J.; Stupp, S. I., 25th Anniversary Article: Supramolecular Materials for Regenerative Medicine. *Adv. Mater.* **2014**, *26* (11), 1642-1659.
- Webber, M. J.; Langer, R., Drug delivery by supramolecular design. *Chem. Soc. Rev.* **2017**, *46* (21), 6600-6620.
- Freeman, R.; Han, M.; Álvarez, Z.; Lewis, J. A.; Wester, J. R.; Stephanopoulos, N.; McClendon, M. T.; Lynsky, C.; Godbe, J. M.; Sangji, H.; Luijten, E.; Stupp, S. I., Reversible self-assembly of superstructured networks. *Science* **2018**, *362* (6416), 808-813.
- Merindol, R.; Walther, A., Materials learning from life: concepts for active, adaptive and autonomous molecular systems. *Chem. Soc. Rev.* **2017**, *46* (18), 5588-5619.
- Walther, A., Viewpoint: From Responsive to Adaptive and Interactive Materials and Materials Systems: A Roadmap. *Adv. Mater.* **2020**, *32* (20), 1905111.
- Zhou, J.; Du, X.; Yamagata, N.; Xu, B., Enzyme-Instructed Self-Assembly of Small d-Peptides as a Multiple-Step Process for Selectively Killing Cancer Cells. *J. Am. Chem. Soc.* **2016**, *138* (11), 3813-3823.
- Zhou, J.; Du, X.; Berciu, C.; He, H.; Shi, J.; Nicastro, D.; Xu, B., Enzyme-Instructed Self-Assembly for Spatiotemporal Profiling of the Activities of Alkaline Phosphatases on Live Cells. *Chem.* **2016**, *1* (2), 246-263.
- Sorrenti, A.; Leira-Iglesias, J.; Sato, A.; Hermans, T. M., Non-equilibrium steady states in supramolecular polymerization. *Nat. Commun.* **2017**, *8* (1), 15899.
- Tantakitti, F.; Boekhoven, J.; Wang, X.; Kazantsev, R. V.; Yu, T.; Li, J.; Zhuang, E.; Zandi, R.; Ortony, J. H.; Newcomb, C. J.; Palmer, L. C.; Shekhawat, G. S.; de la Cruz, M. O.; Schatz, G. C.; Stupp, S. I., Energy landscapes and functions of supramolecular systems. *Nat. Mater.* **2016**, *15* (4), 469-76.
- Hagan, M. F.; Elrad, O. M.; Jack, R. L., Mechanisms of kinetic trapping in self-assembly and phase transformation. *J. Chem. Phys.* **2011**, *135* (10), 104115.
- Nakagawa, M.; Kai, S.; Kojima, T.; Hiraoka, S., Energy-Landscape-Independent Kinetic Trap of an Incomplete Cage in the Self-Assembly of a Pd2L4 Cage. *Chem. Eur. J.* **2018**, *24* (35), 8804-8808.
- Rieß, B.; Grötsch, R. K.; Boekhoven, J., The Design of Dissipative Molecular Assemblies Driven by Chemical Reaction Cycles. *Chem.* **2020**, *6* (3), 552-578.
- Das, K.; Gabrielli, L.; Prins, L. J., Chemically Fueled Self-Assembly in Biology and Chemistry. *Angew. Chem. Int. Ed.* **2021**, *60* (37), 20120-20143.
- Weißenfels, M.; Gemen, J.; Klajn, R., Dissipative Self-Assembly: Fueling with Chemicals versus Light. *Chem.* **2021**, *7* (1), 23-37.
- van Rossum, S. A. P.; Tena-Solsona, M.; van Esch, J. H.; Eelkema, R.; Boekhoven, J., Dissipative out-of-equilibrium assembly of man-made supramolecular materials. *Chem. Soc. Rev.* **2017**, *46* (18), 5519-5535.
- Boekhoven, J.; Hendriksen, W. E.; Koper, G. J. M.; Eelkema, R.; Esch, J. H. v., Transient assembly of active materials fueled by a chemical reaction. *Science* **2015**, *349* (6252), 1075-1079.
- Leira-Iglesias, J.; Tassoni, A.; Adachi, T.; Stich, M.; Hermans, T. M., Oscillations, travelling fronts and patterns in a supramolecular system. *Nat. Nanotechnol.* **2018**, *13* (11), 1021-1027.
- Panja, S.; Dietrich, B.; Adams, D. J., Chemically Fuelled Self-Regulating Gel-to-Gel Transition. *Chem. Systems Chem.* **2020**, *2* (1), e1900038.
- Tena-Solsona, M.; Rieß, B.; Grötsch, R. K.; Löhner, F. C.; Wanzke, C.; Käs Dorf, B.; Bausch, A. R.; Müller-Buschbaum, P.; Lieleg, O.; Boekhoven, J., Non-equilibrium dissipative supramolecular materials with a tunable lifetime. *Nat. Commun.* **2017**, *8* (1), 15895.
- Grötsch, R. K.; Angi, A.; Mideksa, Y. G.; Wanzke, C.; Tena-Solsona, M.; Feige, M. J.; Rieger, B.; Boekhoven, J., Dissipative Self-Assembly of Photoluminescent Silicon Nanocrystals. *Angew. Chem. Int. Ed.* **2018**, *57* (44), 14608-14612.
- Donau, C.; Späth, F.; Sosson, M.; Kriebisch, B. A. K.; Schnitter, F.; Tena-Solsona, M.; Kang, H.-S.; Salibi, E.; Sattler, M.; Mutschler, H.; Boekhoven, J., Active coacervate droplets as a model for membraneless organelles and protocells. *Nat. Commun.* **2020**, *11* (1), 5167.
- Kriebisch, B. A. K.; Jussupow, A.; Bergmann, A. M.; Kohler, F.; Dietz, H.; Kaila, V. R. I.; Boekhoven, J., Reciprocal Coupling in Chemically Fueled Assembly: A Reaction Cycle Regulates Self-Assembly and Vice

- Versa. *J. Am. Chem. Soc.* **2020**, *142* (49), 20837-20844.
30. Wanzke, C.; Jussupow, A.; Kohler, F.; Dietz, H.; Kaila, V. R. I.; Boekhoven, J., Dynamic Vesicles Formed By Dissipative Self-Assembly. *Chem. Systems Chem.* **2020**, *2* (1), e1900044.
31. Dai, K.; Fores, J. R.; Wanzke, C.; Winkeljann, B.; Bergmann, A. M.; Lieleg, O.; Boekhoven, J., Regulating Chemically Fueled Peptide Assemblies by Molecular Design. *J. Am. Chem. Soc.* **2020**, *142* (33), 14142-14149.
32. Boekhoven, J.; Poolman, J. M.; Maity, C.; Li, F.; van der Mee, L.; Minkenberg, C. B.; Mendes, E.; van Esch, J. H.; Eelkema, R., Catalytic control over supramolecular gel formation. *Nat. Chem.* **2013**, *5* (5), 433-437.
33. Hossain, M. M.; Atkinson, J. L.; Hartley, C. S., Dissipative Assembly of Macrocycles Comprising Multiple Transient Bonds. *Angew. Chem. Int. Ed.* **2020**, *59* (33), 13807-13813.
34. Kariyawasam, L. S.; Kron, J. C.; Jiang, R.; Sommer, A. J.; Hartley, C. S., Structure–Property Effects in the Generation of Transient Aqueous Benzoic Acid Anhydrides by Carbodiimide Fuels. *J. Org. Chem.* **2020**, *85* (2), 682-690.
35. Kariyawasam, L. S.; Hartley, C. S., Dissipative Assembly of Aqueous Carboxylic Acid Anhydrides Fueled by Carbodiimides. *J. Am. Chem. Soc.* **2017**, *139* (34), 11949-11955.
36. Schwarz, P. S.; Tena-Solsona, M.; Dai, K.; Boekhoven, J., Carbodiimide-fueled catalytic reaction cycles to regulate supramolecular processes. *Chem. Comm.* **2022**, *58* (9), 1284-1297.
37. Zeng, W.; Fan, C.; Xing, X.; Cheng, H.; Fu, H.; Ma, B.; Yang, Z.; Zhang, R.; Zhang, W., Out of equilibrium coil-helix transition driven by chemical fuels. *Giant* **2021**, *7*, 100067.
38. Singh, N.; Lopez-Acosta, A.; Formon, G. J. M.; Hermans, T. M., Chemically Fueled Self-Sorted Hydrogels. *J. Am. Chem. Soc.* **2022**, *144* (1), 410-415.
39. Kriebisch, C. M. E.; Bergmann, A. M.; Boekhoven, J., Fuel-Driven Dynamic Combinatorial Libraries. *J. Am. Chem. Soc.* **2021**, *143* (20), 7719-7725.
40. Bal, S.; Ghosh, C.; Ghosh, T.; Vijayaraghavan, R. K.; Das, D., Non-Equilibrium Polymerization of Cross- $\beta$  Amyloid Peptides for Temporal Control of Electronic Properties. *Angew. Chem. Int. Ed.* **2020**, *59* (32), 13506-13510.
41. Bal, S.; Das, K.; Ahmed, S.; Das, D., Chemically Fueled Dissipative Self-Assembly that Exploits Cooperative Catalysis. *Angew. Chem. Int. Ed.* **2019**, *58* (1), 244-247.
42. Tena-Solsona, M.; Wanzke, C.; Riess, B.; Bausch, A. R.; Boekhoven, J., Self-selection of dissipative assemblies driven by primitive chemical reaction networks. *Nat. Commun.* **2018**, *9* (1), 2044.
43. Dai, K.; Tena-Solsona, M.; Rodon Fores, J.; Bergmann, A. M.; Boekhoven, J., Morphological transitions in chemically fueled self-assembly. *Nanoscale* **2021**, *13* (47), 19864-19869.
44. Panzarasa, G.; Torzynski, A. L.; Sai, T.; Smith-Mannschott, K.; Dufresne, E. R., Transient supramolecular assembly of a functional perylene diimide controlled by a programmable pH cycle. *Soft Matter* **2020**, *16* (3), 591-594.
45. Schnitter, F.; Boekhoven, J., A Method to Quench Carbodiimide-Fueled Self-Assembly. *Chem. Systems Chem.* **2021**, *3* (1), e2000037.
46. Wang, Y.; Lovrak, M.; Liu, Q.; Maity, C.; le Sage, V. A. A.; Guo, X.; Eelkema, R.; van Esch, J. H., Hierarchically Compartmentalized Supramolecular Gels through Multilevel Self-Sorting. *J. Am. Chem. Soc.* **2019**, *141* (7), 2847-2851.
47. Harris, T. K.; Turner, G. J., Structural Basis of Perturbed pKa Values of Catalytic Groups in Enzyme Active Sites. *IUBMB Life* **2002**, *53* (2), 85-98.
48. Tang, C.; Smith, A. M.; Collins, R. F.; Ulijn, R. V.; Saiani, A., Fmoc-diphenylalanine self-assembly mechanism induces apparent pKa shifts. *Langmuir* **2009**, *25* (16), 9447-53.
49. Richardson, J. S.; Richardson, D. C., Natural  $\beta$ -sheet proteins use negative design to avoid edge-to-edge aggregation. *PNAS* **2002**, *99* (5), 2754.
50. Stsiapura, V. I.; Maskevich, A. A.; Kuzmitsky, V. A.; Turoverov, K. K.; Kuznetsova, I. M., Computational Study of Thioflavin T Torsional Relaxation in the Excited State. *J. Phys. Chem. A* **2007**, *111* (22), 4829-4835.
51. Kubelka, J.; Keiderling, T. A., Differentiation of  $\beta$ -Sheet-Forming Structures: Ab Initio-Based Simulations of IR Absorption and Vibrational CD for Model Peptide and Protein  $\beta$ -Sheets. *J. Am. Chem. Soc.* **2001**, *123* (48), 12048-12058.
52. Krimm, S.; Bandekar, J., Vibrational spectroscopy and conformation of peptides, polypeptides, and proteins. *Adv. Protein Chem.* **1986**, *38*, 181-364.
53. Cheng, G.; Castelletto, V.; Moulton, C. M.; Newby, G. E.; Hamley, I. W., Hydrogelation and Self-Assembly of Fmoc-Tripeptides: Unexpected Influence of Sequence on Self-Assembled Fibril Structure, and Hydrogel Modulus and Anisotropy. *Langmuir* **2010**, *26* (7), 4990-4998.

TOC:

